NeuroImage 63 (2012) 553–568

Contents lists available at SciVerse ScienceDirect

NeuroImage

journal homepage: www.elsevier.com/locate/ynimg

Detection of event-related hemodynamic response to neuroactivation by dynamic modeling of brain activity

Muhammad Aqil [a], Keum-Shik Hong [a,b,*], Myung-Yung Jeong [a], Shuzhi Sam Ge [a,c]

[a] Department of Cogno-Mechatronics Engineering, Pusan National University, 30 Jangjeon-dong, Geumjeong-gu, Busan 609-735, Republic of Korea
[b] School of Mechanical Engineering, Pusan National University, 30 Jangjeon-dong, Geumjeong-gu, Busan 609-735, Republic of Korea
[c] Department of Electrical and Computer Engineering, National University of Singapore, Singapore 117576, Singapore

ARTICLE INFO

Article history:
Accepted 6 July 2012
Available online 14 July 2012

Keywords:
Dynamic modeling of brain activity
State-space model
Real-time brain imaging
Near-infrared spectroscopy (NIRS)
Brain–computer interface (BCI)

ABSTRACT

This paper presents a state-space hemodynamic model by which any event-related hemodynamic prediction function (i.e., the basis function of the design matrix in the general linear model) is obtained as an output of the model. To model the actual event-related behavior during a task period (intra-activity dynamics) besides the contrasting behavior among the different task periods and against the rest periods (inter-activity dynamics), the modular system is investigated by parametric subspace-based state-space modeling of actual hemodynamic response to an impulse stimulus. This model provides a simple and computationally efficient way to generate the event-related basis function for an experiment by just convolving the developed hemodynamic model with the impulse approximation of the experimental stimuli. The demonstration of the stated findings is carried out by conducting finger-related experiments with slow- and fast-sampling near-infrared spectroscopy instruments to model and validate the cortical hemodynamic responses. The generated basis functions of the finger-related experiments are adapted from real data to validate the incorporation of non-delayed and real-time event-related features and to effectively demonstrate a dynamic-modeling-based online framework. The proposed method demonstrates potential in estimating event-related intra- and inter-activation dynamics and thereby outperforms the classical Gaussian approximation method.

Introduction

Functional near-infrared spectroscopy (fNIRS), a noninvasive optical imaging method, detects brain activation by measuring the concentration changes of oxygenated (oxi) and de-oxygenated (doxy) hemoglobins (HbO and HbR, respectively) in blood corpuscles representing activity in nearby neurons (Aqil et al., 2012; Bunce et al., 2006; Cope and Delpy, 1988; Cui et al., 2010a; Hu et al., 2010, 2011, 2012; Plichta et al., 2007, 2011). Nowadays, the general linear model (GLM)-based approach to signal processing in brain activation areas is common, especially for functional magnetic resonance imaging (fMRI)- and fNIRS-based technologies (Cui et al., 2011; Friston et al., 2008; Ye et al., 2009), due to its robustness even in the cases of incorrect differential path length factors (DPF) (Zhao et al., 2002) and severe optical signal attenuation. The GLM approach totally relies on the prediction (basis) function, which combines with its dispersion derivatives to form the feature (activity dynamics) extracting design matrix. The conventional approach to obtaining the basis function convolves a canonical hemodynamic response (HR) with the experimental stimuli of the targeting experiment, whereas the canonical HR, taken to be the response of oxi-hemoglobin to a pulsed stimulus, is approximated as a Gaussian curve and the experimental stimuli are approximated as a box-car function (see Abdelnour and Huppert, 2009; Cui et al., 2011; Friston et al., 2008; Ye et al., 2009 and references therein). By utilizing a unique canonical HR or its approximation function (Gaussian approximation) as a response for any stimuli, which is not the case in reality (Luo and Puthusserypady, 2007), the existing method ignores the actual event-related behavior during a task period (intra-activity dynamics) inherent to the performing task, inserts a delay between the modeling of the expected activity and the actual occurrence of the event, and effectively suppresses the event-related features to be modeled for peer recursive extraction. Hence, the method hardly affects maximum-likelihood-based offline studies for detection of the contrasting behavior among the different task periods and against the rest periods (inter-activation dynamics), but is cumbersome for real-time event-related hemodynamic studies.

Poor dynamic modeling, coupled with offline-restricted feature extraction of associated parameters, is a bottleneck to the achievement of event-related applications, like brain–computer interface (BCI) and brain–machine interface (BMI) systems. This obstacle needs to be surmounted instead of avoided. Researchers paid due attention, to some extent, to this problem. Markham et al. (2009) carried out an offline study for blind identification of brain activity

* Corresponding author at: Department of Cogno-Mechatronics Engineering, Pusan National University, 30 Jangjeon-dong, Geumjeong-gu, Busan 609-735, Republic of Korea. Fax: +82 51 514 0685.
E-mail addresses: aqil@pusan.ac.kr (M. Aqil), kshong@pusan.ac.kr (K.-S. Hong), myjeong@pusan.ac.kr (M.-Y. Jeong), samge@nus.edu.sg (S.S. Ge).

1053-8119/$ – see front matter © 2012 Elsevier Inc. All rights reserved.
doi:10.1016/j.neuroimage.2012.07.006

with optical signals; Li et al. (2010) determined nonparametric slow drift fMRI signals by Fourier representation of the classical HR functions with the possibilities of occurrence of false-positive errors; and Hinds et al. (2011) recursively computed moment-to-moment HRs by an incremental GLM. All of these methods, however, are restricted to the detection of activated brain regions and inter-activation dynamics. Also, dynamic-model-based investigations have been carried out to address the hemodynamic strength for the fMRI modality (Makni et al., 2008; Penny et al., 2005), but such methods are also limited to offline detection of the activated brain region. In addressing event-related dynamics, Cui et al. (2010b) and Hu et al. (2011) demonstrated the possibility of a fast optical response, but with extensive offline processing (the averaging of several sessions of a particular task) due to the too-weak signal. Rapid event-related designs, introduced to parameterize and detect the different contrast/intensity levels of a task, provide efficient ways of addressing the inter-activity task levels (see for example Plichta et al., 2007 and references therein). Most of the aforementioned methods impose further conditions regarding the duration and repeatability of the same activation task to enhance robustness.

Motor-related cortical activations are the most useful approaches to BCI control (Matthews et al., 2008). Recently, some contributions were reported in the capacity of online or, somehow, real-time fNIRS-BCI applications to estimate the parameters of a GLM as coefficients of a recursive least squares filter (Aqil et al., 2012) or states of a Kalman filter (Abdelnour and Huppert, 2009; Hu et al., 2010). However, these approaches to detection of blocks of active periods still lack dynamical information on intra-activation blocks. These limitations, significantly, restrict their capacity to just online methodologies in addressing tasks' blocks. The event-related utilities, like BCI and BMI applications, require an effective solution to these problems.

In order to overcome these limitations while deriving an event-related hemodynamic prediction function, we investigate a new approach, as per our knowledge, involving dynamic modeling of the HR, stimulus input vs. hemodynamic output (Aqil et al., 2011b). The demonstration of the stated findings is carried out by conducting finger-related experiments with slow- and fast-sampling fNIRS instruments to model and validate the cortical hemodynamic responses. Parametric subspace-based state-space modeling is performed to avoid most of the *a priori* parameterization. The method is advantageous in providing a dynamic model directly in the form of state-space matrices with optimally conditioned and uniquely determined bases (thereby avoiding the identifiability problem) (Ljung, 2008; Overschee and Moor, 1994; Viberg, 2002). The proposed hemodynamic model facilitates the obtainment of basis functions, incorporating the event-related intra-activation dynamics, for any experiment related to the modeled brain region by convolving the proposed model with the impulse approximation of the experimental stimuli. The proposed hemodynamic-model-based approach provides better results than the classical method, due to its dynamic behavior for both fast- and slow-switching stimuli. The proposed model utilizes the skills learned for activation behavior (start, stop, and peaking) of the impulse HR instead of using a unique HR or its approximating function. A comparative analysis against the classical method is performed, involving demonstration of the typical steps for designing experimental stimuli and obtaining the basis functions for two validating experiments. The experiments are designed to test the applicability of the proposed strategy for i) the motor cortex regions, ii) the variability of the tasking pace, iii) the null-control events, iv) the slow- and fast-sampled datasets, and v) testing the periodic repeated consistency (to signify the robustness of the statistical testing) of a regional brain task. The proposed method is found to outperform the classical method by preserving information on the event-related brain activity (intra-activation dynamics) in addition to that on the brain activity status (inter-activation dynamics). The proposed basis function with respect to the capacity to address non-delayed event-related features is further validated by utilizing recursive least-square (RLS)- and Kalman filtering (KF)-based adaptive frameworks from our previous papers (Aqil et al., 2012; Hu et al., 2010), respectively, to effectively demonstrate the dynamic-modeling-based online platform. The statistical significance of the experimental results is evaluated with *t*-statistics and interpolated brain activation maps are drawn to localize the activity region. The method can be utilized to model any brain region. The main contributions of this paper are the following: i) a dynamic model is proposed to address the event-related hemodynamic response. ii) The proposed model provides, for any experiment, the simple and computationally efficient means of generating a basis function and of incorporating the event-related intra- and inter-activation dynamics for a cortical brain task. iii) The generated basis function avoids modeling delay, and effectively enhances the event-related features that are to be extracted recursively during event-related applications, like BCI and BMI systems.

This paper is organized as follows. The Theory section describes the computational approach to dynamic modeling of the cortical HR and to obtaining the basis function for targeting validation experiments followed by the description of RLS- and KF-based adaptive frameworks. The Method section details experimental protocol for obtaining the cortical HR for the peer modeling process, and for validation of the model's capability of generating the event-related hemodynamic basis. The Results and discussion section demonstrates and discusses the effectiveness of the modeling-based approach to obtaining event-related basis functions for the targeting physiological experiments verified by estimating the predicted features from the real data with adaptive frameworks. Finally, concluding remarks are provided in the Conclusions section.

Theory

Identification model for cortical hemodynamic response

A multivariable system can conveniently be described, in terms of state-space representation (Aqil et al., 2011a; Rehan et al., 2011), as

$$\begin{aligned} z(k+1) &= Az(k) + Bu(k) + w(k), \\ x(k) &= Cz(k) + Du(k) + \varepsilon(k), \end{aligned} \tag{1}$$

where $z(k)$ denotes the modeling states, $x(k)$ is the desired hemodynamic output, $u(k)$ is the stimulus input, $w(k)$ is the unobservable disturbance input, $\varepsilon(k)$ is the additive noise, k is the discrete time index, and $A \in \Re^{p\times p}$, $B \in \Re^{p\times 1}$, $C \in \Re^{1\times p}$, and $D \in \Re^{1\times 1}$ represent the coefficient matrices with p as the number of modular states to be chosen optimally.

To model the hemodynamic response, subspace-based state-space modeling is performed for an impulse–response dataset $\{u(k), x(k)\}$ consisting of the input impulse stimuli and the resulting cortical hemodynamic response. For γ successive samples of the impulse–response dataset of form $\Psi_x(k) = [x(k) \quad x(k+1) \quad \cdots \quad x(k+\gamma-1)]$ and $\Psi_u(k) = [u(k) \quad u(k+1) \quad \cdots \quad u(k+\gamma-1)]$ with $\gamma > p$, the algebraic formulation (1) can be rewritten as (Ljung, 2008; Overschee and Moor, 1994; Viberg, 2002)

$$\Psi_x(k) = \Gamma z(k) + \Phi \Psi_u(k) + n(k), \tag{2}$$

where $\Gamma \in \Re^{\gamma\times p}$ is the extended observability matrix, $\Phi \in \Re^{\gamma\times\gamma}$ is a block lower triangular Toeplitz matrix containing impulse–response coefficients, and $n(k)$ represents the noise contribution, which is supposed

to be white Gaussian with zero mean. The extended observability matrix and block triangular Toeplitz matrix have the forms

$$\Gamma = \begin{bmatrix} C & CA & \cdots & CA^{\gamma-1} \end{bmatrix}^T \tag{3}$$

and

$$\Phi = \begin{bmatrix} D & 0 & \cdots & 0 & 0 \\ CB & D & \ddots & 0 & 0 \\ \vdots & \ddots & \ddots & 0 & 0 \\ \vdots & & & & \vdots \\ CA^{\gamma-2}B & CA^{\gamma-3}B & \cdots & CB & D \end{bmatrix}. \tag{4}$$

The superscript T is the transpose operator. The extended observability matrix spans the signal subspace, and is extracted from the impulse–response dataset. There are many ways to extract subspace system identification. The projection method, like the least-square method, is followed to estimate the extended observability matrix by correlating both sides of Eq. (2) with quantities that eliminate the term $\Psi_u(k)$, and making the noise influence $n(k)$ disappear asymptotically (Ljung, 2008; Overschee and Moor, 1994; Viberg, 2002). Once Γ is estimated, matrix C is projected directly from the first block row, and the A matrix is found by exploiting the shift-invariance structure of the extended observability relation (3). The remaining matrices B and D are then calculated by a linear least squares from

$$x(k) = C(q\mathbf{I} - A)^{-1}Bu(k) + Du(k), \tag{5}$$

where q is the eigenvalue of the state matrix A. It is worth noting that subspace-based state-space modeling is performed to avoid most of the *a priori* parameterization. The method is advantageous in providing the dynamic model directly as full state-space matrices on an optimally conditioned and uniquely determined basis (thereby avoiding the identifiability problem). Thus, the issue of unknown observability (or controllability) indices can be addressed equally well. Furthermore, the absence of any nonlinear optimizing component makes it, unlike other algorithms, undisruptive in the face of disadvantages such as local minima, unsure convergence, and sensitivity to initial estimates. Also, it is insensitive to initial states, even zero initial states (Overschee and Moor, 1994).

Estimation of prediction (basis) function

The potential output response to an input, of course, can be estimated by exciting (convolving) the identified impulse–response model with the input. It is here proposed, therefore, that the event-related basis function for any experiment can be obtained as $x(k)$ simply by exciting (convolving) the investigated dynamic HR model with the pulse-train representation of the experimental stimuli as $u(k)$. The proposed hemodynamic-model-based approach of obtaining the basis function requires matrix (having minimal order) manipulations instead of dealing with the entries of long canonical-HR vector (containing the sampled version of the canonical HR). Despite using the convolution process, the proposed model-based estimation can be realized efficiently through the Control System Toolbox of MATLAB®, either with script-m-file or with the Simulink approach, to simulate the time responses of the dynamic model to arbitrary inputs. Thus, the proposed approach is simple. Moreover, the proposed methodology is computationally efficient as it requires fewer computations and memory space than the canonical HR-based convolution.

The Results and discussion section below will demonstrate the proposed basis estimation method in the light of two targeting experiments, and then will detail its validation by adaptive frameworks with experimental data from fNIRS instruments.

Brain activation model

Measurement model for fNIRS: modified Beer–Lambert law (MBLL)

The concentration changes of HbX (i.e., HbO and HbR), Δc_{HbX} in μM, using the MBLL (Cope and Delpy, 1988) are given by

$$\begin{bmatrix} \Delta\phi^i_{\mathrm{HbO}}(t) \\ \Delta\phi^i_{\mathrm{HbR}}(t) \end{bmatrix} = \begin{bmatrix} a_{\mathrm{HbO}}(\lambda_1) & a_{\mathrm{HbR}}(\lambda_1) \\ a_{\mathrm{HbO}}(\lambda_2) & a_{\mathrm{HbR}}(\lambda_2) \end{bmatrix}^{-1} \begin{bmatrix} \Delta\phi^i(t;\ \lambda_1) \\ \Delta\phi^i(t;\ \lambda_2) \end{bmatrix}, \tag{6a}$$

$$\Delta c^i_{\mathrm{HbX}}(t) = \frac{\Delta\phi^i_{\mathrm{HbX}}(t)}{d^i l^i}, \tag{6b}$$

where the superscript i ($i = 1, 2, \ldots, M$) denotes the i-th measuring channel of the source and detector pair, M denotes the total number of channels, $\Delta\phi^i_{\mathrm{HbX}}(t)$ is the optical density variation of HbX in μM·mm at the i-th channel, $\Delta\phi^i(t;\lambda_j)$ ($j = 1,2$) is the unitless total optical density variation of the light source of wavelength λ_j, $a_{\mathrm{HbX}}(\lambda_j)$ is the extinction coefficient of HbX in $\mu M^{-1}\cdot mm^{-1}$, d^i is the unitless DPF, and l^i is the distance (in millimeters) between the source and the detector at the i-th channel. The formulated MBLL (Eqs. (6a) and (6b)) is equally applicable for continuous-wave (CW) and frequency-domain (FD) fNIRS instruments once the absorption parameter is determined by their respective theories. It is worth noting that FD-fNIRS provides concentrations of HbO and HbR i) on the absolute scale by solving Boltzmann's transport equation for absorption and reduced-scattering coefficients, if utilized in multi-distance configuration (Fantini et al., 1999); and ii) on a relative scale (similar to CW-fNIRS), if utilized in spatially distributed source–detector configuration (Gallagher et al., 2008; Machado et al., 2011; Stankovic et al., 1999). The second configuration is followed in this study to cover a wide measuring range.

Activation model

In this section, a linear model to identify the area of activation for a targeting experiment is introduced. For the measured HbO concentration $y^i(t) =^{\Delta} \Delta c^i_{\mathrm{HbO}}(k)$, the proposed discrete linear model is defined as

$$\begin{aligned} y^i(k) &= x_1(k)\beta^i_1(k) + x_2(k)\beta^i_2(k) + \cdots + x_m(k)\beta^i_m(k) + v^i(k) \\ &= X^T(k)\beta^i(k) + v^i(k), \end{aligned} \tag{7}$$

where $X(k) = [x_1(k) \quad x_2(k) \quad \cdots \quad x_m(k)]^T$ is the k-th sample vector of m regression (prediction or basis) functions, $\beta^i(k) = \begin{bmatrix} \beta^i_1(k) & \beta^i_2(k) & \cdots & \beta^i_m(k) \end{bmatrix}^T$ is the slowly varying parameters representing the activity strength corresponding to the m regression functions at channel i (to be estimated), and $v(k) \sim (0, R)$ denotes the observation noise at channel i.

There are many ways of designing the predicting regressor functions (like parametric or factorial models) to evaluate the appropriate tests of interests. A parametric regression modeling (expected HR as linear and continuous functions of the stimuli pattern) is followed to address i) the relationship of the levels (contrast) of the activity events (Friston et al., 2008), ii) the recursive assessment of statistical significance by testing the null hypothesis for both activity and null control by means of repeated measurements, and iii) the real-time treatment of each subject's scan (within-subject testing) independently to demonstrate the potential for BCI/BMI applications. Although the actual HR model is developed independently for each subject, the first and second temporal derivatives of the HR are included as the regressor functions to address the time varying HR's latency and dispersion (Friston et al., 2008; Plichta et al., 2007). A separate no-stimulus regressor is included to test the null control (Plichta et al., 2007). The no-stimulus regressor is obtained by convolving the no-stimulus pattern, having a value of 1 during the no-stimulus periods (including the null control and rest periods) and 0 otherwise (Friston et al., 2008).

Thus, the proposed regressor vector $X(k)$ in this study consists of the sampled version of the proposed linear parametric activity

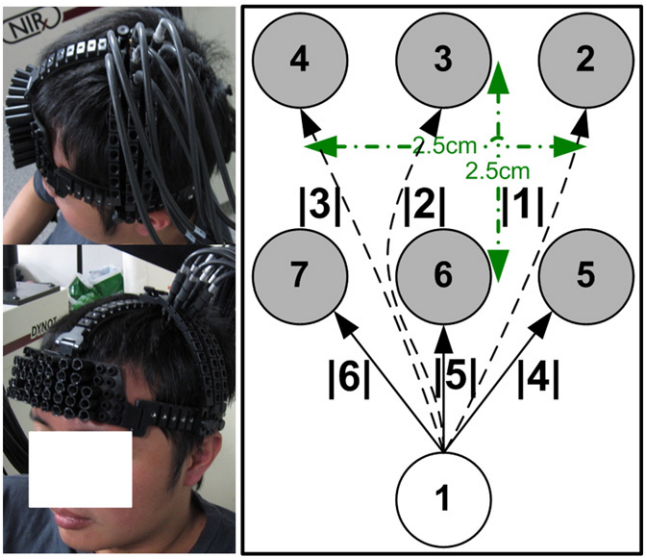

Fig. 1. Channel configuration (single source, fast sampling) for cortical HR investigation: Six channels with one source (circle # 1) and six detectors (circles # 2–# 7).

prediction function $x(k)$ as $x_1(k)$, its two derivatives $\Delta x(k)$ and $\Delta^2 x(k)$ as $x_2(k)$ and $x_3(k)$, respectively, a null control regressor as $x_4(k)$, and an offset. The activity strength vector at all channels, $\beta^i(k)$, can be adapted recursively for a run-time platform.

Recursive least-squares (RLS) estimation: This estimator computes the temporal statistics directly at each time-step to determine the optimal filter coefficients by minimizing the square of the error of the estimated and model responses (Haykin, 2002). The RLS estimation of the single-channel activity model (7) translates into finding the parameter vector $\hat{\beta}^i(k)$ as (Aqil et al., 2012)

$$e^i(k) = y^i(k) - \hat{y}^i(k), \tag{8}$$

$$\hat{\beta}^i(k) = \hat{\beta}^i(k-1) + K(k)e^i(k), \tag{9}$$

$$K(k) = P(k-1)X(k)\left(1 + X^{\mathrm{T}}(k)P(k-1)X(k)\right)^{-1}, \tag{10}$$

$$P(k) = \left(I - K(k)X^{\mathrm{T}}(k)\right)P(k-1), \tag{11}$$

where $e^i(k)$ is the estimation error, $\hat{y}^i(k) = X^{\mathrm{T}}(k)\hat{\beta}^i(k-1)$ is the estimated sample of the modeled event-related output, $K(k) \in \Re^{5\times 1}$ is the weighting vector for parameter updating, and $P(k) \in \Re^{5\times 5}$ is the input covariance matrix at sample-time k. In the present study, the state vector $\beta^i(k)$ and the input covariance matrix $P(k)$ are initialized to zero and δI, $\delta = 10$, respectively.

Kalman filter (KF): The Kalman filter estimates the state of the process using an updated regularized linear inversion routine (Haykin, 2002; Hu et al., 2010). In the present study, the KF is used to recursively estimate the coefficients $\beta^i(k)$ of the brain activation model (7). For this formulation, the single-channel transition equation can be described in the form

$$\beta^i(k) = \hat{\beta}^i(k-1) + \eta(k), \tag{12}$$

where the state matrix is considered as an identity matrix, and the process noise as $\eta(k) \sim (0, Q)$ to follow a random walk with zero drift over time. The KF based iterative state estimation (12) of the single-channel activity model (7) translates into

$$\Theta^-(k) = \Theta(k-1) + Q, \tag{13}$$

$$K(k) = \Theta^-(k)X(k)E^{-1}(k), \tag{14}$$

$$\hat{\beta}^i(k) = \hat{\beta}^i(k-1) + K(k)e^i(k), \tag{15}$$

$$\Theta(k) = \left(I - K(k)X^T(k)\right)\Theta^-(k), \tag{16}$$

where the superscript $(-)$ refers to the intermediate prediction of the quantities before being updated by the measured data, $E(k) = X^T(k)\Theta^-(k)X(k) + R$, $e^i(k) = y(k) - \hat{y}^i(k)$ as defined in Eq. (8), $K(k) \in \Re^{5\times 1}$ is again the weighting vector (called Kalman gain here) for parameter updating, and $\Theta(k) \in \Re^{5\times 5}$ is the updated error covariance matrix. In the present study, the state vector $\beta^i(k)$ is initialized to zero, and the *a priori* process and observation noise covariances (Q and R) are found to be $(1\%/\mathrm{s})^2$ and $(0.5\ \mu\mathrm{M/s})^2$, respectively.

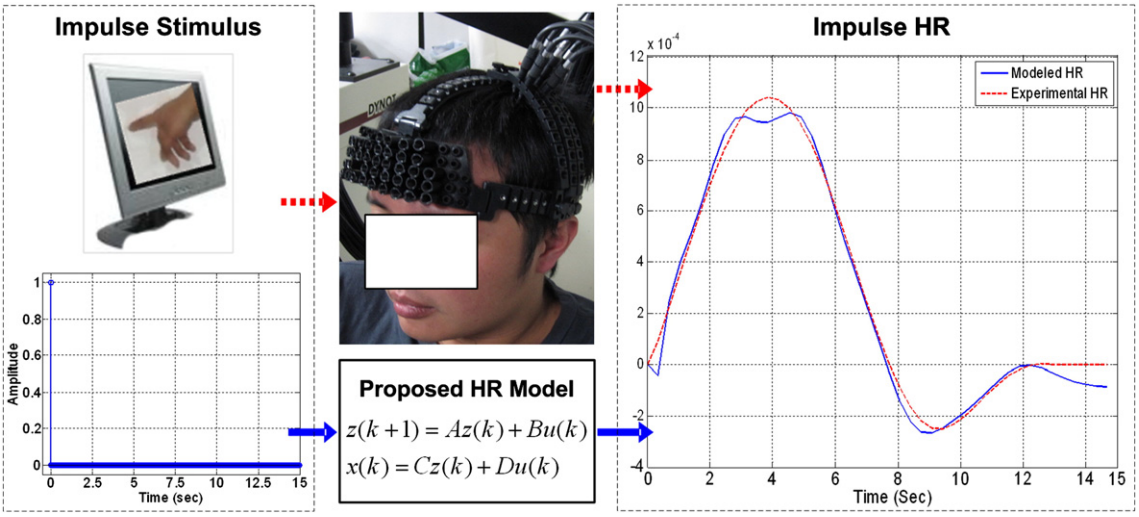

Fig. 2. The experimentally obtained hemodynamic response (dotted curve) vs. the impulse response of the proposed state-space model (1) (solid curve).

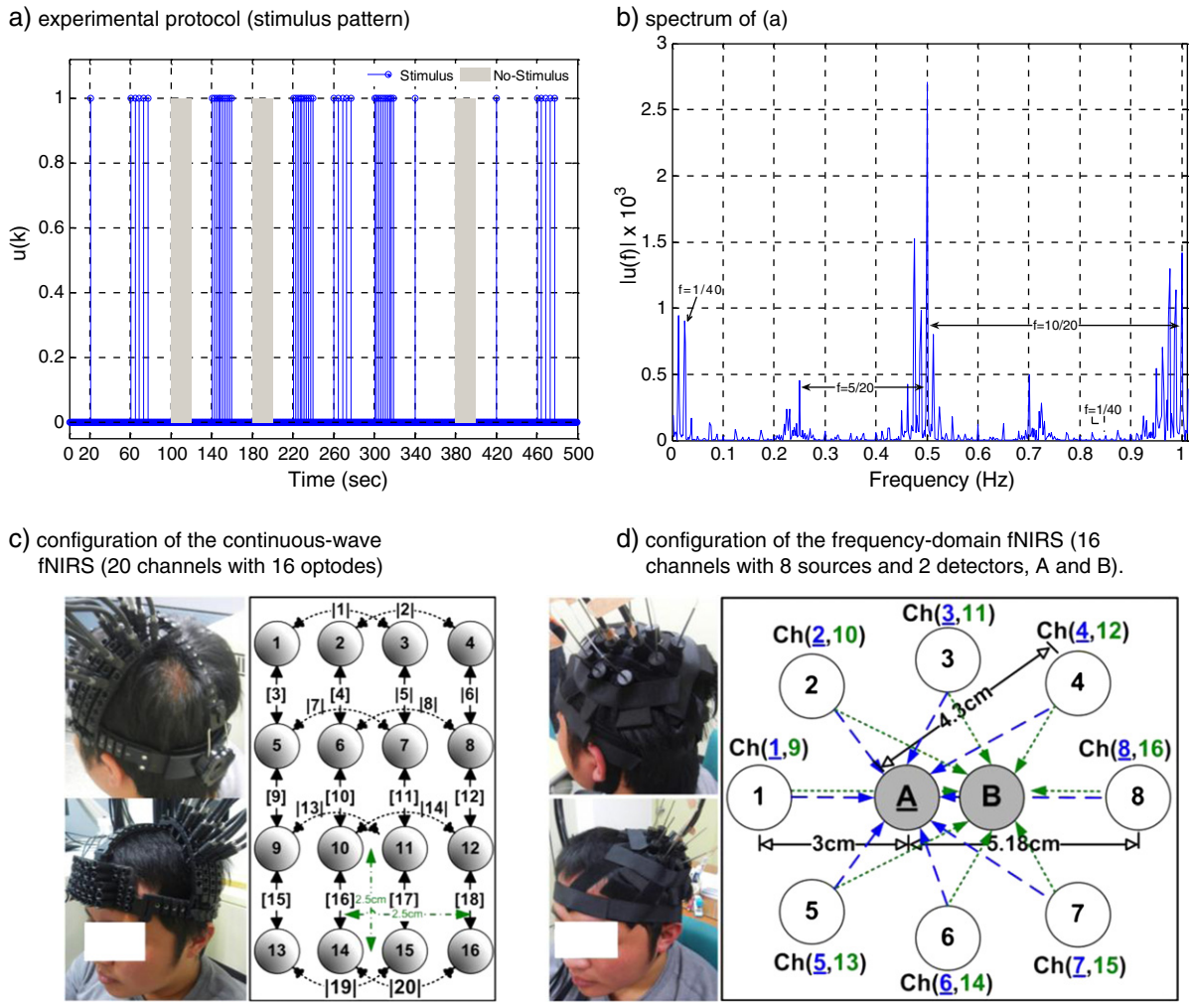

Fig. 3. Experimental setup for the variable-pace RIFT experiment.

Activation mapping

Although the MBLL formulation (Eqs. (6a) and (6b)) is used extensively, this is merely a first-order approximation of diffusive light scattering (see for example the photon path described in Boas et al., 1997). The Rytov approximation by O'Leary et al. (1995) provides a solution for estimating the HbX changes at any position r within the measuring range by the interpolation relation

$$\Delta c_{\mathrm{HbX}}(t,\ r) = \sum_{i=1}^{M} b^i(r)\Delta\phi^i_{\mathrm{HbX}}(t), \tag{17}$$

where $b^i(r)$ corresponds to the interpolation kernel derived from the diffusion equation (i.e., the spatial correlation with the adjacent channels' hemoglobin status) (Boas et al., 1997). The interpolated activity strength $\hat{\alpha}(k,r)$ at time k is obtained as

$$\hat{\alpha}(k,r) = \left(B^T(r)\otimes I_5\right)\hat{\beta}(k) \tag{18}$$

where $B(r)$ is the stacking vector of interpolation kernels given by

$$B(r) = \left[\, b^1(r) \quad b^2(r) \quad \cdots \quad b^M(r) \,\right] \tag{19}$$

and $\otimes$ is the Kronecker product. The corresponding error covariance is

$$C_{\hat{\alpha}}(k,r) = \left(B^T(r)\Sigma B(r)\right)\otimes\left(X^{+}\Lambda X^{+T}\right), \tag{20}$$

where $\Sigma = diag(\sigma_1^2(k),\sigma_2^2(k),\cdots,\sigma_M^2)$ with σ_i^2 being the residual sum-of-squares divided by the appropriate degrees of freedom at channel i, the superscript $+$ denotes the pseudo inverse operator, X is the stacking form of the regressor vector $X(k)$, and Λ is the common temporal correlation matrix for all the channels ($\Lambda = I$ is used in this paper).

Statistical significance

The statistical significance of the estimated activity parameter $\hat{\beta}^i(k)$, test of the null hypothesis $c^T\hat{\beta}^i(k) = 0$, is evaluated by one-tailed t-test (t-statistics) at time-step k and location r as (Aqil et al., 2012)

$$t_{\hat{\beta}}(r,k) = \frac{c^T\hat{\alpha}(r,k)}{\sqrt{\left(B^T(r)\Sigma B(r)\right)\left(c^T X^{+}\Lambda X^{+T}c\right)}}, \tag{21}$$

where c represents a contrast vector for selecting the parameter(s) of interest. Thus, the null hypothesis is assessed by a t-distribution with $k-L$ degrees of freedom, where L is the number of regressors. It is noteworthy that the statistical significance of the activity parameter is ensuring the statistical significance of the modeled event-related

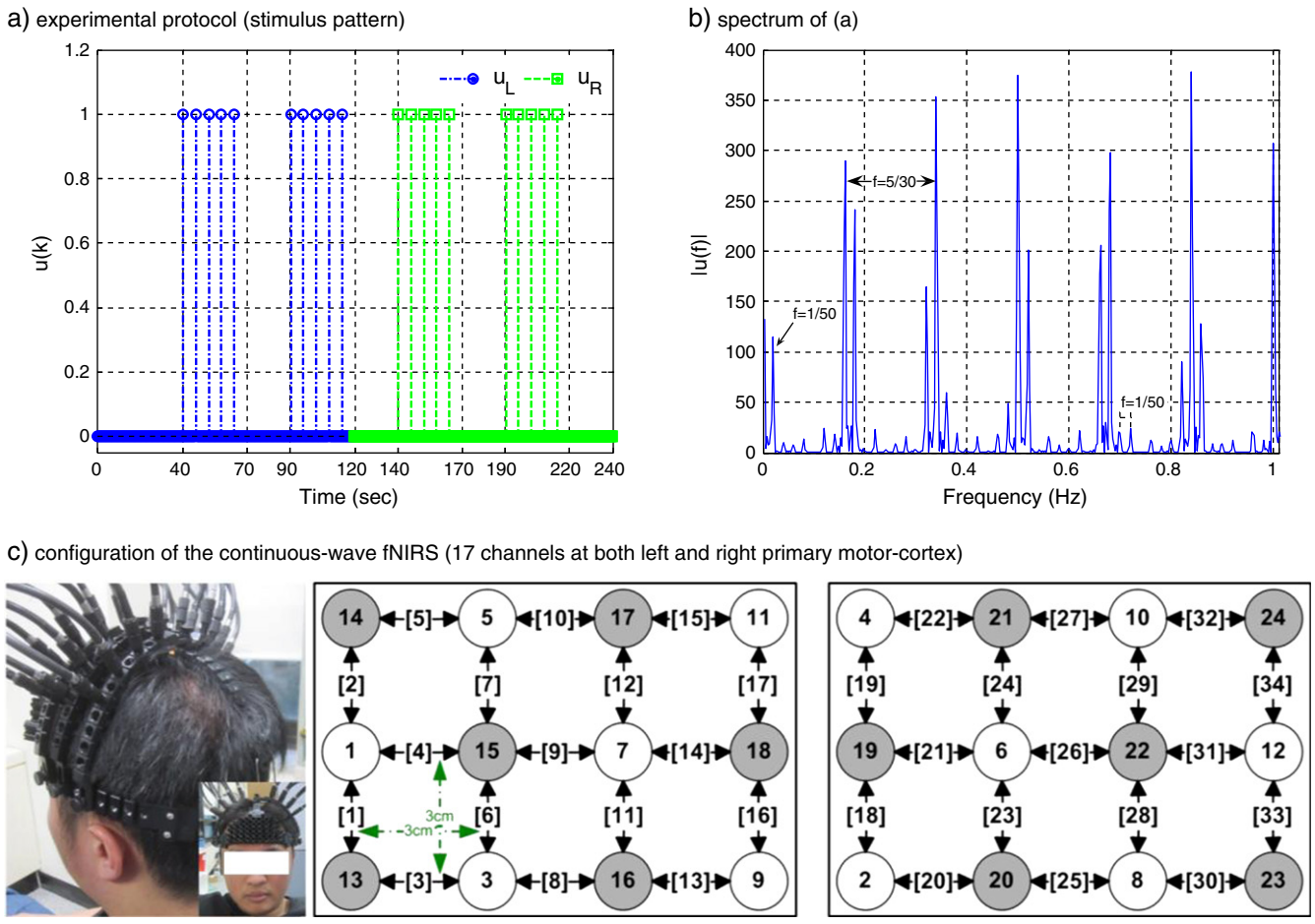

Fig. 4. Experimental setup for the MCFG experiment.

output, which is estimated as $\hat{y}^i(k) = X^T(k)\hat{\beta}^i(k-1)$ from a real dataset by RLS and KF estimators.

Method

Since a finger task, covering the dominant area of the motor cortex, is known to elicit a robust hemodynamic response, finger-related tasks are preferred. The experimental protocols for obtaining the cortical HR for the peer modeling process and for validation of the model's capability of generating the event-related hemodynamic basis are as follows.

Investigation of cortical HR to impulse stimulus

Behavioral experiments are conducted using the fNIRS modality to obtain actual hemodynamic activity at the cortical surface against an impulse stimulus. A two-wavelength (760 nm and 830 nm) CW-fNIRS instrument (DYNOT; NIRx Medical Technologies, USA) is used in the single-source fast-run configuration. The fast run (fast sampling) configuration is chosen in order to incorporate the fast dynamics for event-related modeling, large frequency band for an appropriate filtering process, and large data points for a precise and smooth model identification process. Six measuring channels are configured with one source and six detectors, as shown in Fig. 1. The specific behavioral protocol of the experiment consisted of an initial 20 s for signal equilibrium followed by three sessions of 40 s duration each. The subjects are instructed to perform right-index finger tapping (RIFT) once at the start of each session, which is followed by a rest period. For each subject, the time series of active channels are preprocessed (low-pass filter with Gaussian function having a FWHM of 1.5 s, high-pass filter with discrete-cosine transform having a cutoff of 128 s, and the baseline is corrected to initial time) and then averaged over the experiments and over the task sessions to obtain the actual HR for an impulse stimulus. A schematic diagram illustrating the comprehensive HR-modeling framework is provided in Fig. 2. The dotted curve shows the experimentally investigated cortical HR (averaged) of subject 1 to a single RIFT stimulus. For intra-activity dynamics modeling, the mathematical form of the single-tap stimulus is approximated as an impulse function, shown at the bottom left of Fig. 2, to effectively attain an impulse–stimulus HR dataset $\{u(k),x(k)\}$.

The Results and discussion section will outline the stated theoretical steps in obtaining the dynamic-HR model by utilizing this actual HR dataset followed by its validation. To appreciate the model's potential for obtaining the basis function for targeting experiments and in addressing the event-related dynamics of brain tasks, we consider the behavioral protocol of validating experiments and configurations of the fNIRS measuring instruments in the following subsection.

Variable-pace RIFT experiment

A variable-pace RIFT experiment is designed to test the applicability of the proposed strategy in terms of i) the motor cortex activity, ii) the variability of the tasking pace, iii) the null-control events, and iv) the slow- and fast-sampled datasets. The behavioral protocol consists of a

a) a box-car type function (representing the experimental protocol) is convolved with the classical HR

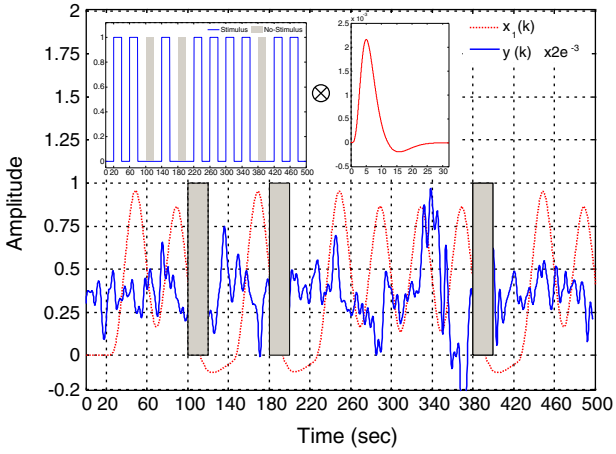

d) the spectrum of $\chi_1(\kappa)$ in (a)

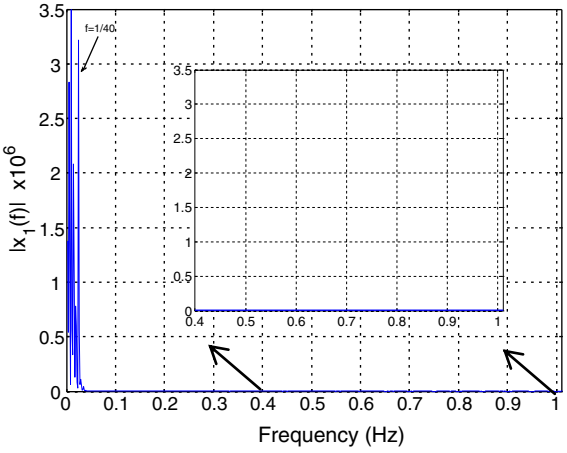

b) the impulse stimuli (representing the experimental protocol) are convolved with the classical HR

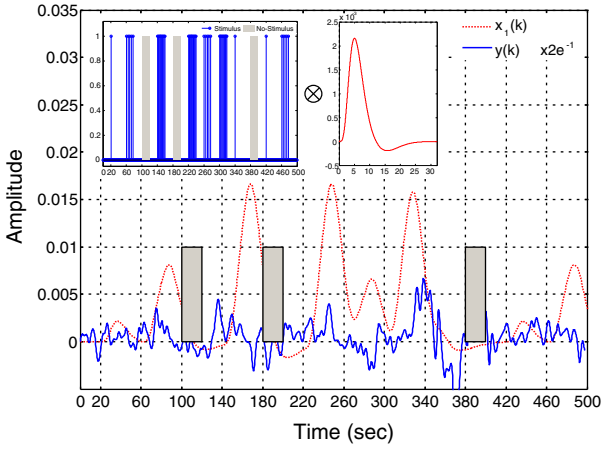

e) the spectrum of $\chi_1(\kappa)$ in (b)

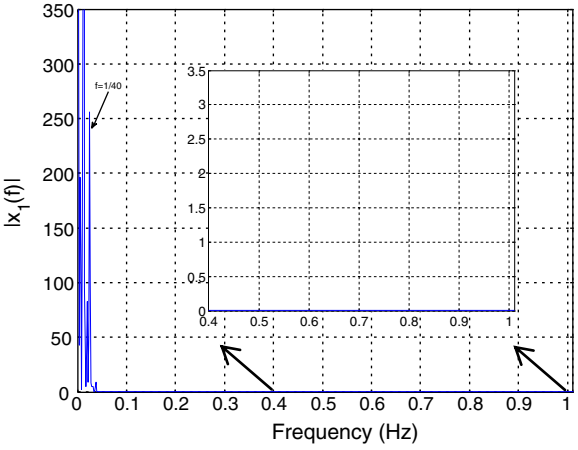

c) the impulse stimuli are convolved with the proposed state-space model.

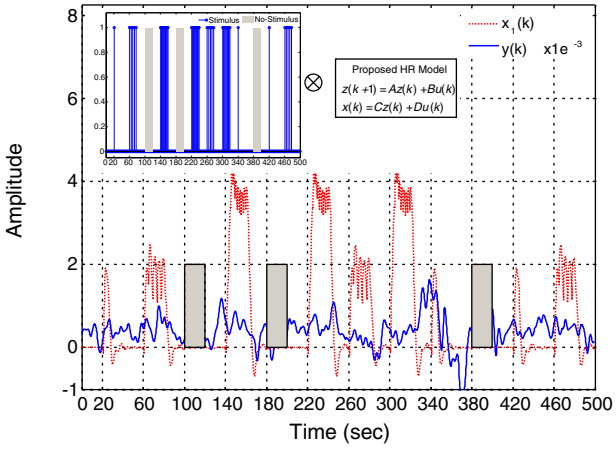

f) the spectrum of $\chi_1(\kappa)$ in (c)

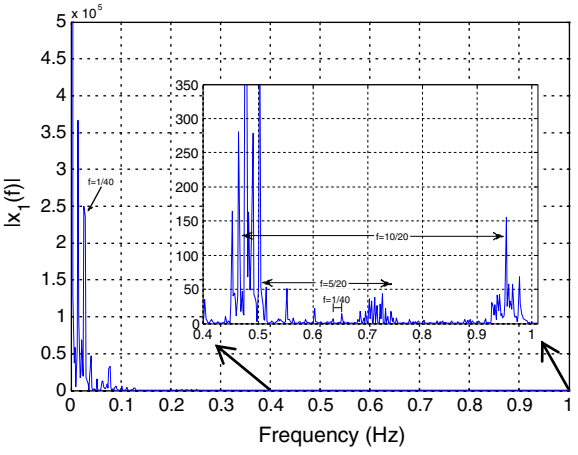

Fig. 5. Comparison of three basis functions, $x_1(k)$, for the variable-pace RIFT experiment (plotted with the actual HR $y(k)$ measured at an active channel).

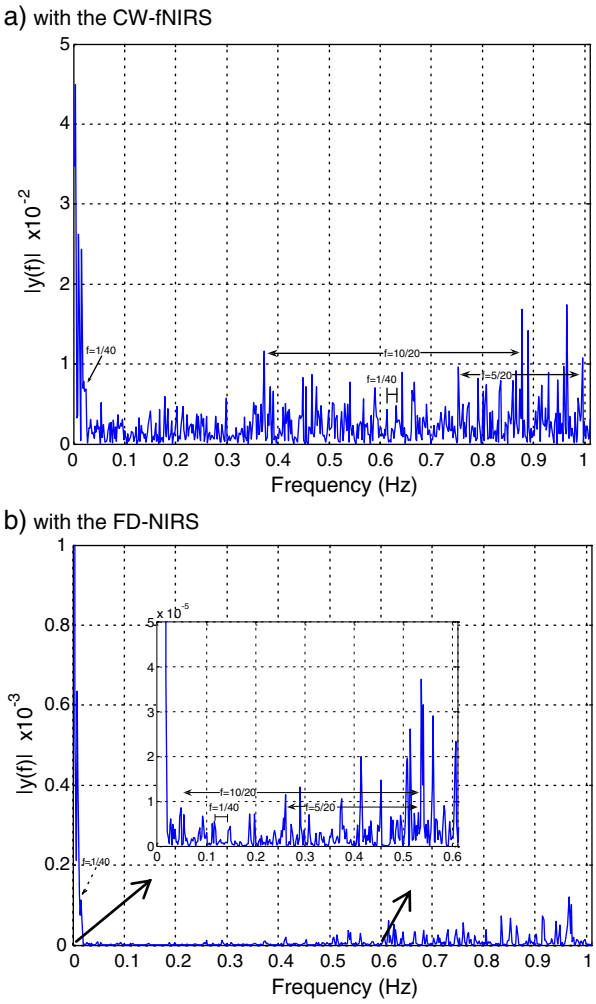

Fig. 6. Spectrum of the actual HR signals, $y(k)$, observed at an active channel during the variable-pace RIFT experiment.

20 s initial rest for signal stability, followed by twelve sessions of 40 s duration each. One of the three differently paced (1-, 5-, and 10-tapping) RIFT task stimuli or a null control stimuli is presented during the first 20 s of a session. The three predefined paced tapping tasks enable us to validate the modeling of the intra activity dynamics of the performing tasks. Each of the four (three differently paced tapping and a null control) stimuli sessions is presented three times in a predetermined pseudorandom order (consistency of the same stimuli is avoided). The subjects are instructed to tap once during the 1-tap sessions, five times during the 5-tap sessions, and ten times during the 10-tap sessions, all at the specific times commanded through the animated- and parallel-port-interrupted-GUI. The center fixation cross was constantly presented during the whole experiment (with the exception of the commanded tap events during the three tapping tasks) to avoid subjects' concentration/focus and motion artifacts. Since the occurrence of three different tapping contrast and null-control sessions is unpredictable for a subject, the rest period is varying (21 to 79 s, average: 50 s) in nature which avoids the subject' adaptability to a higher extent. The predetermined randomized impulse representation of the behavioral protocol is plotted in Fig. 3(a) along with its rich frequency spectrum, shown in Fig. 3(b), consisting of three kinds of infinite pulses separated by 1/40, 5/20, and 10/20 Hz, as per the tapping frequencies. The session frequency is also 1/40 Hz.

CW-fNIRS instrument

The two-wavelength (760 nm and 830 nm) CW-fNIRS (DYNOT; NIRx Medical Technologies, USA) instrument is configured for twenty measuring channels with sixteen optodes (co-located source–detector pairs) to cover the left motor cortex, as shown in Fig. 3(c). The sampling rate is 2.86 Hz. The experiment is carried out twice for three male subjects of age 28 ± 3 years, and the detected optical density variations are converted to concentration changes of oxi and doxy hemoglobins by utilizing the MBLL, and then preprocessed (low-pass filter with Gaussian function having a FWHM of 1.5 s, high-pass filter with discrete-cosine transform having a cutoff of 128 s, and baseline is corrected to initial time).

FD-fNIRS instrument

A two-wavelength (690 nm and 830 nm) FD-fNIRS instrument (Imagent; ISS, Inc., USA) with sensor-pad channel configuration (sixteen measuring channels) to cover the left motor cortex, see Fig. 3(d), is employed to probe the optical density variations due to oxi and doxi hemoglobin concentration changes over the left motor cortex. The sampling rate is 15.625 Hz. Again, the experiment is carried out twice for three male subjects of age 28 ± 3 years. The detected optical density variations are converted to concentration changes of oxi and doxy hemoglobins, and then preprocessed in a similar way for comparison.

Multi-cortex finger-grasping experiment

The multi-cortex finger-grasping (MCFG) experiment is designed to further validate the method for two different regions of a brain (left and right motor cortexes) by means of periodic repeated consistency (to signify the robustness of the statistical testing) of a regional task over time besides testing the applicability in terms of i) motor cortex activity, ii) the event related task, and iii) the null-control events. The experiment consists of a 40 s signal equilibrium period followed by four sessions of 50 s each. All sessions comprise a 30 s task and a 20 s rest period. The subjects are instructed to perform the finger grasping task five times with the specified hand during the task periods at time instants specified via a GUI. The first two sessions correspond to the consistent right hand's grasping task (to activate the left motor cortex) and, simultaneously, serve as the consistent null control sessions of the left hand task. Similarly, the last two sessions correspond to the left hand's grasping task (to activate the right motor cortex) and, simultaneously, serve as the null control sessions of the right hand task. Fig. 4(a) shows the stimuli pattern for left and right motor cortexes as u_L and u_R, respectively. The frequency spectrum of the stimuli, plotted in Fig. 4(b), consists of two kinds of infinite pulses separated by 1/50 and 5/30 Hz as per the tapping and session frequencies. Fig. 4(c) shows the channel configuration of CW-NIRS instrument to measure signals from the left and right motor cortexes. The experiment is carried out twice for three male subjects of age 28 ± 3 years. The optical density variations, detected at a sampling rate of 2.86 Hz, are converted to concentration changes of oxi and doxy hemoglobins by utilizing the MBLL, and then preprocessed in a similar way for comparison.

Results and discussion

Identification of dynamic HR model

Parameter matrices of the proposed state-space model (1) are adapted by minimizing the prediction error cost function and the state sequences are determined by the projection of the obtained input–output dataset, which is plotted in Fig. 2 (dotted curve). Order six is found to be optimal in modeling the cortical HR, the impulse excitation of which approximately replicates the practically

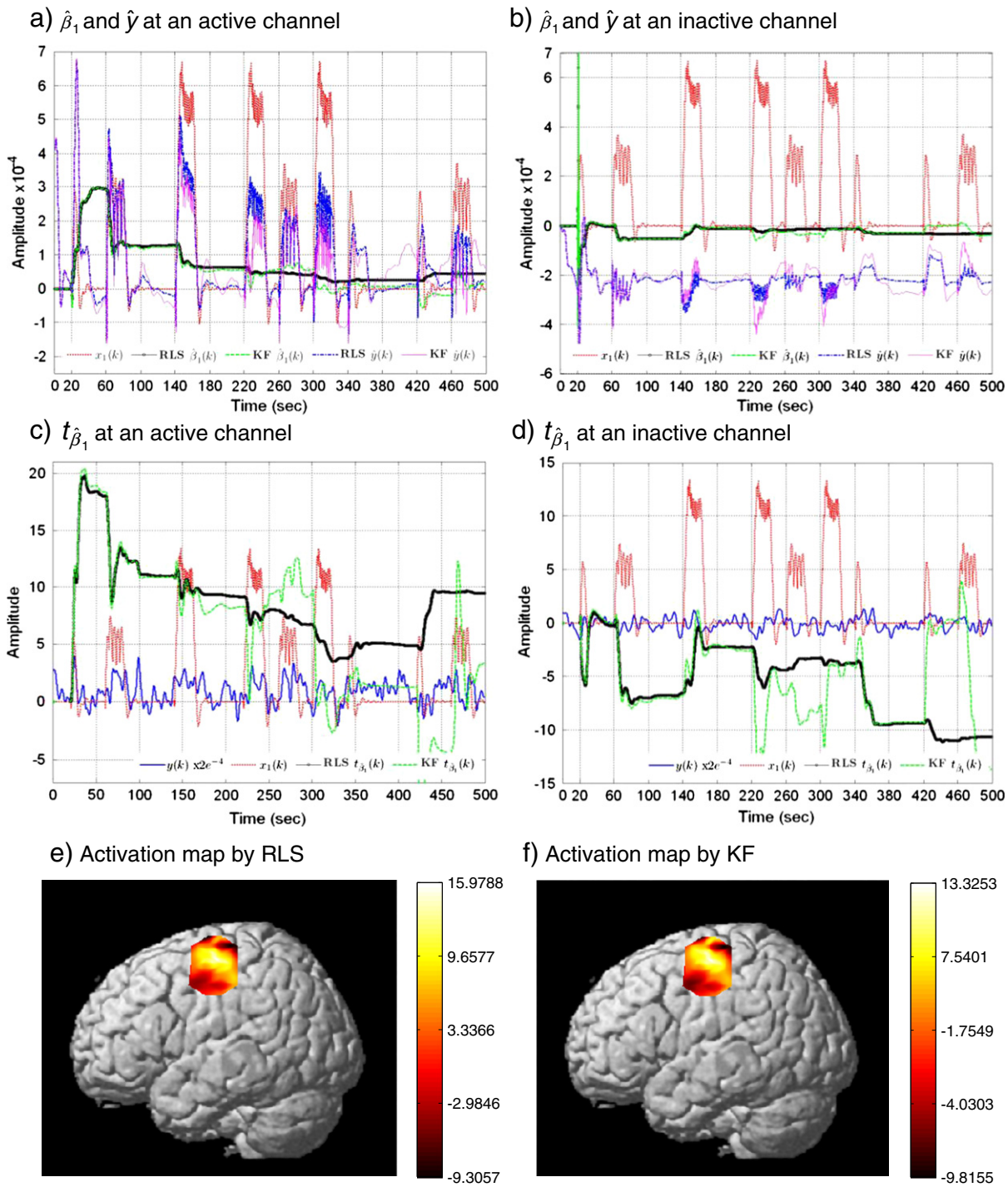

Fig. 7. Results of the variable-pace RIFT experiment conducted with the CW-fNIRS: (a)–(b) recursively extracted activity parameter $\hat{\beta}_1(k)$ and estimated output $\hat{y}(k)$ along with the appropriately scaled modeled response $x_1(k)$; (c)–(d) statistical significance (t-scores) of activity parameter, $t_{\hat{\beta}_1}(k)$, along with the modeled response $x_1(k)$ and the real response $y(k)$ observed at that channel; (e)–(f) brain activation maps drawn after the convergence of the activity parameters.

investigated HR, as shown in Fig. 2 (solid curve). This completes the first task: modeling of cortical HR for fNIRS modality.

Validation results via RIFT experiment

Basis function for validating experiment

Classical approach: The basis function obtained by the classical method, that is, by convolving the experiment's stimuli with the Gaussian-approximated HR vector, is shown in Fig. 5(a) along with the actual HR signal $y(k)$ measured at an active channel. As per the method's requirements, the stimulus input is approximated as a box-car function (a constant step-value during the whole tasking period, 20 s here), and the sampling rate is altered to ten times faster than the actual sampling frequency of the conducting experiment. It is clear from the plot that the conventional method does not provide the dynamic information on the event-related hemodynamic activity. Unlike a box-car approximation of the experimental stimulus, an impulse-train approximation is found to be useless (see Fig. 5(b)) for indicating the activity dynamics (there is

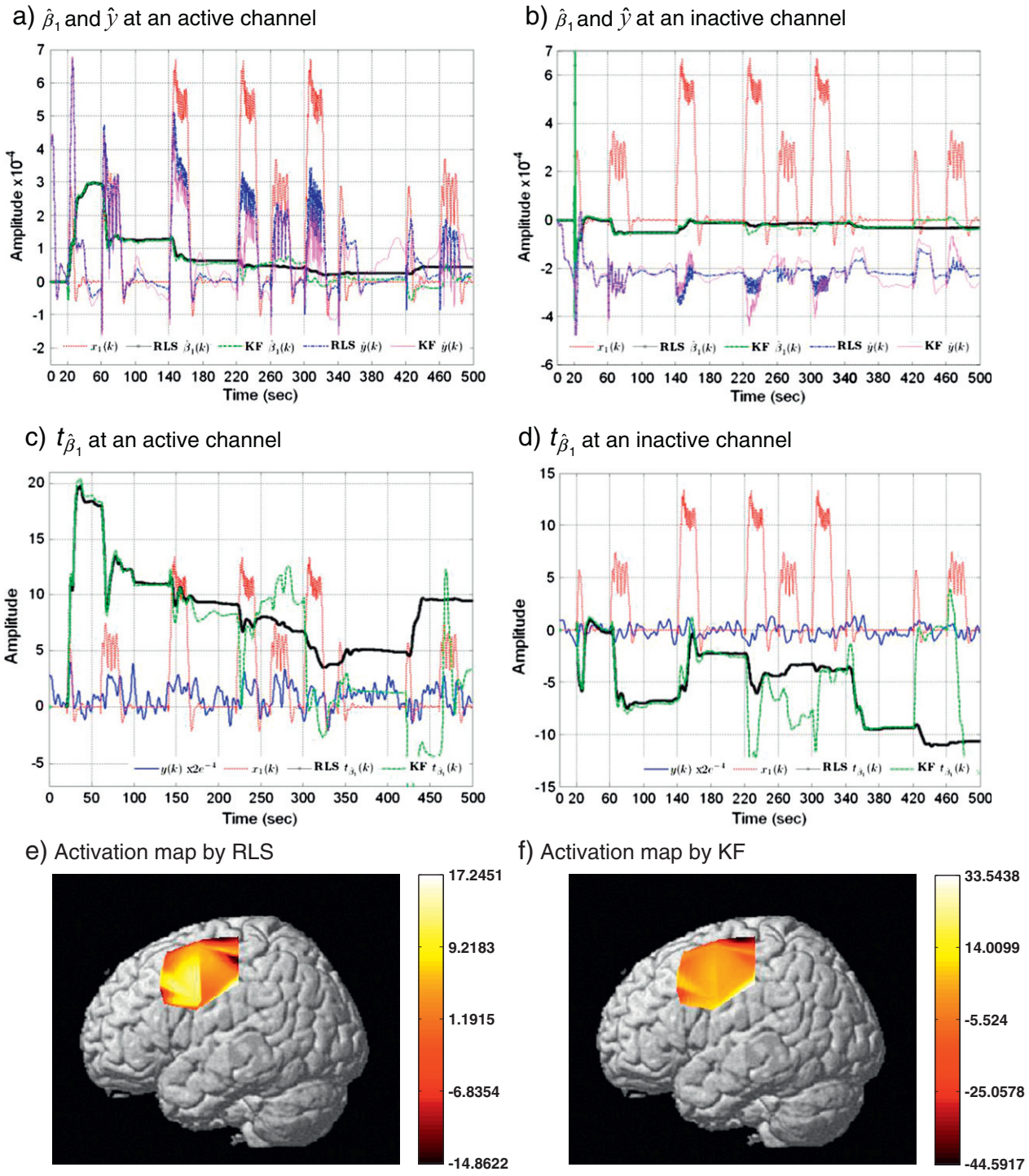

Fig. 8. Results of the variable-pace RIFT experiment conducted with the FD-fNIRS: (a)–(b) recursively extracted activity parameter $\hat{\beta}_1(k)$ and estimated output $\hat{y}(k)$ along with the appropriately scaled modeled response $x_1(k)$; (c)–(d) statistical significance (t-scores) of activity parameter, $t_{\hat{\beta}_1}(k)$, along with the modeled response $x_1(k)$ and the real response $y(k)$ observed at that channel; (e)–(f) brain activation maps drawn after the convergence of the activity parameters.

no intra-activity-block information), and is corrupted by a delayed indication of the activity blocks (delayed inter-activity-block information). In both cases, only the task sessions' frequency is detectable, unsurprisingly, due to its periodicity with the rest sessions, which is shown by the frequency responses (Figs. 5(d–e)). Hence, it is clear that the classical method does not inscribe the intra-activity dynamics of a brain task, it rather treats the pace (intra-activity) information as the task intensity information by means of amplitude coding, and thus is of only limited use in applications stressing the activation strength in different brain regions during performance of a task.

Proposed dynamic-model-based approach: The basis function of the targeting variable-pace RIFT experiment obtained by the proposed strategy, plotted in Figs. 5(c,f), addresses the intra-activity dynamics in terms of the superimposed event-related ringing signals (marking the intra-dynamics' frequencies exactly at the targeted tasking frequencies 1/40, 5/20, and 10/20) on top of the low-frequency inter-activation-block signal. On the other hand, though the amplitude of the actually observed HR signal is influenced by different noise sources, the tasking frequencies still can be observed in the frequency spectrums, shown in Fig. 6, of appropriate active channels measured

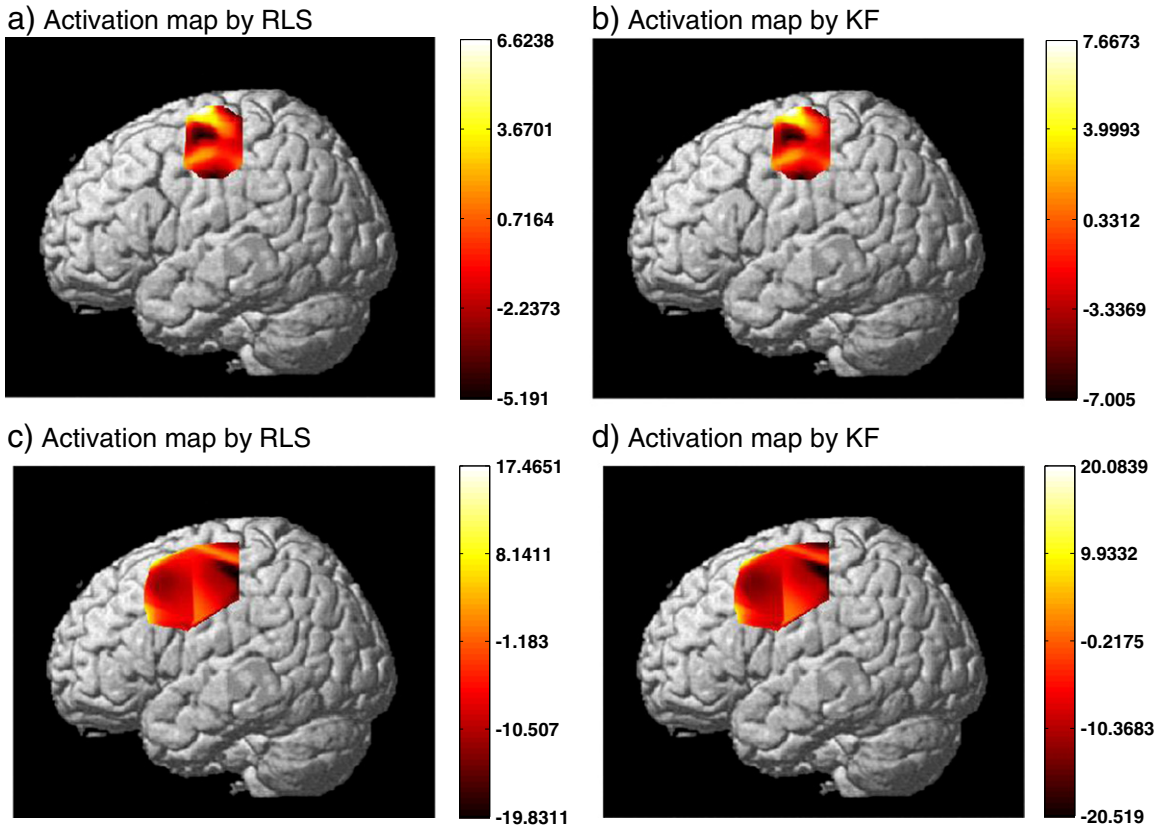

Fig. 9. Activation maps (drawn after the convergence of the activity parameters at the same time instants at which the proposed model based maps have been drawn) by the classical basis function (regressed with RLS and KF methods) for the variable-pace RIFT experiment: (a)–(b) using the CW-fNIRS, (c)–(d) using the FD-fNIRS.

with the CW-fNIRS and FD-NIRS instruments during the experiment. Thus, advantageously, the proposed basis function incorporates the exact stimulation spectrum for potential real-time applications.

It is noteworthy that the proposed hemodynamic model based approach of generating the basis function is simple as compared to the traditional methods. Our method requires matrix (with maximum order p, e.g. $p=6$ was found optimal for the shown validating experiment) manipulations instead of dealing with the entries of long HR-vector (containing the sampled version of the canonical HR). Additionally, the proposed methodology (manipulating model (1) of order 6) is computationally efficient as well because it requires fewer computations and memory space than the conventional approach (handling a canonical HR-vector of order 1032).

Extraction of event-related dynamics from real data

To examine the potential of the proposed basis function in addressing the actual event-related dynamics for validating RIFT experimental datasets, the activity parameter $\hat{\beta}^i(k)$ and the event-related output $\hat{y}^i(k)$ are estimated by the stated RLS- (Eqs. (8)–(11)) and KF-based (Eqs. (13)–(16)) adaptive online frameworks. The activity strength of the modeled HR basis function $\hat{\beta}_1^i(k)$ is analyzed by selecting the contrast vector as $c=[1\ \ 0\ \ 0\ \ 0\ \ 0]^T$. Figs. 7(a) and (b) illustrate the event-related dynamics $\hat{y}^i(k)$ (dash–dot and solid curves by RLS and KF methods, respectively) and corresponding activity strength $\hat{\beta}_1(k)$ (circled and dashed curves by RLS and KF methods, respectively) corresponding to an active and an inactive channel, respectively, for the CW-fNIRS instrument. These results are found statistically significant as evaluated by one-tailed t-test (Eq. (21)) of the activity parameter $\hat{\beta}_1(k)$ ($t_{\hat{\beta}_1}(k)$; dash–dot and dashed curves by RLS and KF methods, respectively) which is plotted in Figs. 7(c–d) along with the real data $y^i(k)$ at the channel i. The interpolated brain activation maps are drawn after the convergence of the activity parameter $\hat{\beta}_1(k)$ estimated by RLS and KF methods as shown in Figs. 7(e–f). Similarly, Figs. 8(a) and (b) demonstrate the event-related dynamics, estimated by RLS and KF methods, corresponding to an active and an inactive channel, respectively, for the FD-fNIRS instrument. Figs. 8(c–d) show the statistical significance of the results obtained with FD-fNIRS instrument plotted along with the real data $y^i(k)$ at the channel i. The interpolated brain activation maps over the range of the FD-NIRS sensors are drawn in Figs. 8(e–f) after the convergence of the activity parameter. The classical basis function based brain activation maps over the full range of measuring channels (obtained with both the fNIRS instruments) are drawn in Fig. 9 for comparison. Note that the t-values from the proposed HR model based basis function are higher than the t-values obtained with the classical basis functions. The reason is that the proposed HR is a better predictor of the actual HR even for varying tasking dynamics.

It should be noted that the first three sessions (single tap periods) verified the experiment's control (the cortical HR, obtained with different experiments, modeled for the prediction function of this experiment) for subject 1. The null control is analyzed by selecting the contrast vector as $c=[0\ \ 0\ \ 0\ \ 1\ \ 0]^T$. Figs. 10(a) and (b) illustrate the null control parameters $\hat{\beta}_4(k)$ (circled and dashed curves by RLS and KF methods, respectively) and respective insignificant t-value ($t_{\hat{\beta}_4}(k)$; dash–dot and solid curves by RLS and KF methods, respectively) corresponding to an active and an inactive channel, respectively, for the CW-fNIRS instrument. Similarly, Figs. 10(c) and (d) demonstrate the null control parameters and respective insignificant t-values, estimated by RLS and KF methods, corresponding to an active and an inactive channel, respectively, for the FD-fNIRS instrument.

The variable-pace RIFT datasets conducted with the CW-fNIRS instrument are further utilized for group analysis. The global alignment-based (between the interpolated maps onto the brain template) group analysis is performed, i.e., the summary statistics of individual subjects is obtained and interpolated first on the global template followed by the across group analysis (Ye et al., 2009).

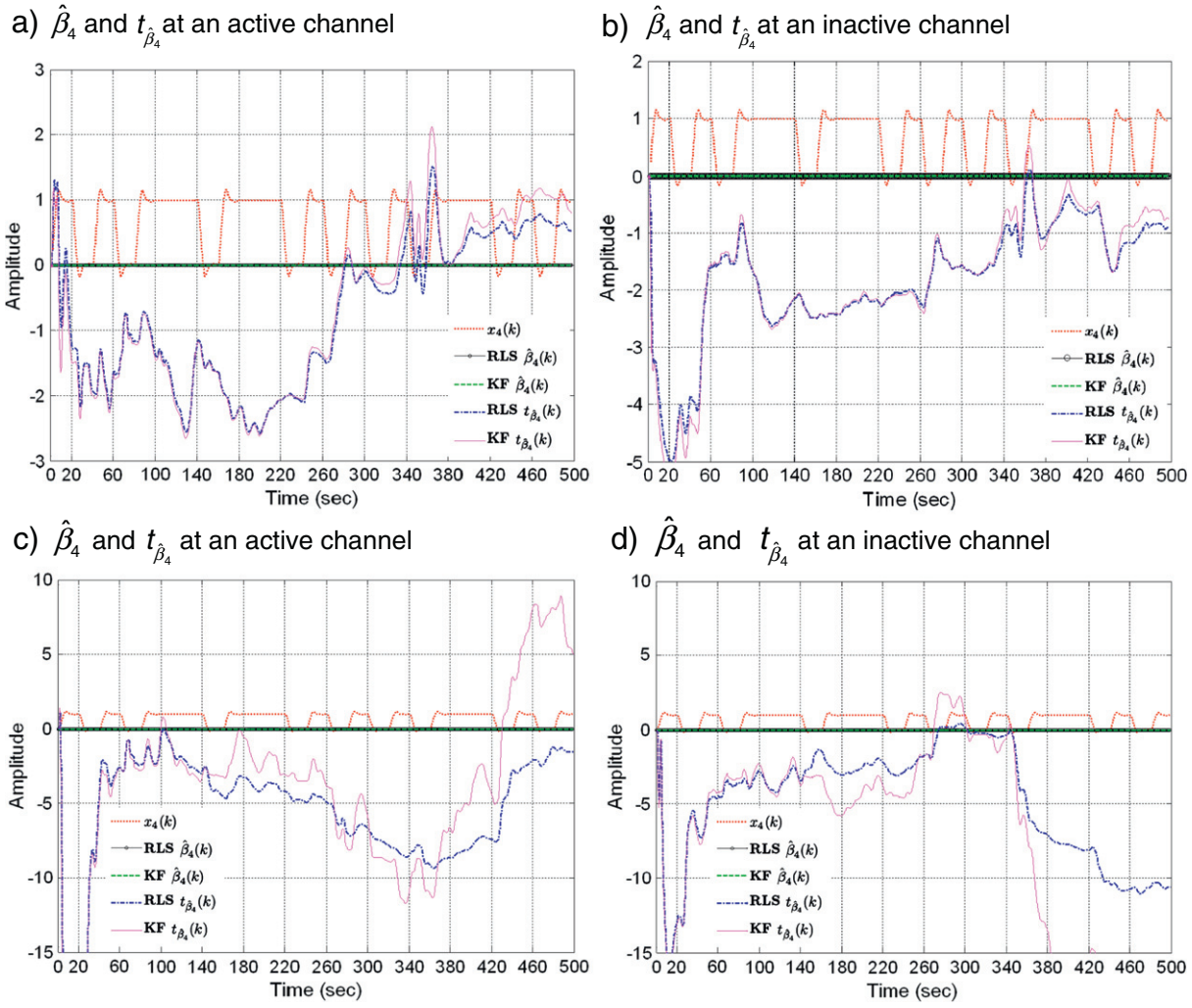

Fig. 10. Null control validation of the variable-pace RIFT experiments: Recursively extracted null control parameter $\hat{\beta}_4(k)$ and respective insignificant t-scores, $t_{\hat{\beta}_4}(k)$, along with the appropriately scaled modeled response $x_1(k)$ at appropriate active and inactive channels: (a)–(b) measured with the CW-fNIRS, (c)–(d) measured with the FD-fNIRS.

Fig. 11 shows the activation maps found by the group analysis using the classical and proposed basis functions regressed with the RLS method. Although there is not much significant difference in time-averaged group activation maps drawn with classical and proposed basis functions, the proposed basis function provides further information (intra-activity behavior) about the performing task. The mesh portrait of the proposed basis function based estimated outputs ($\hat{y}^i(k)$ here), if drawn over all the channels at each time step k, can provide real-time event-related intra-activation pattern, which cannot be obtained with the classical basis function.

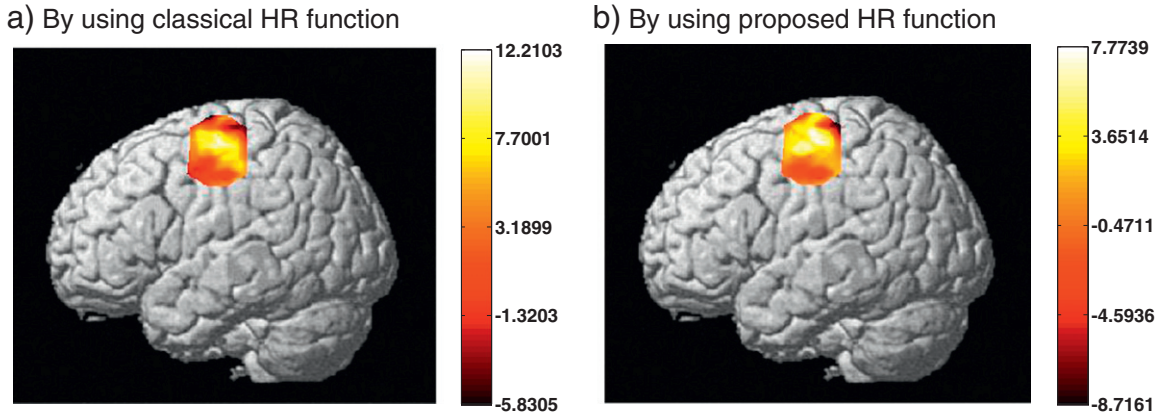

Fig. 11. Activation maps obtained by the group analysis of the variable-pace RIFT experiment, 3 datasets (conducted with the CW-fNIRS only): (a) group activation map found with the classical basis function, (b) group activation map investigated with the proposed basis function. The basis functions are regressed with the RLS method.

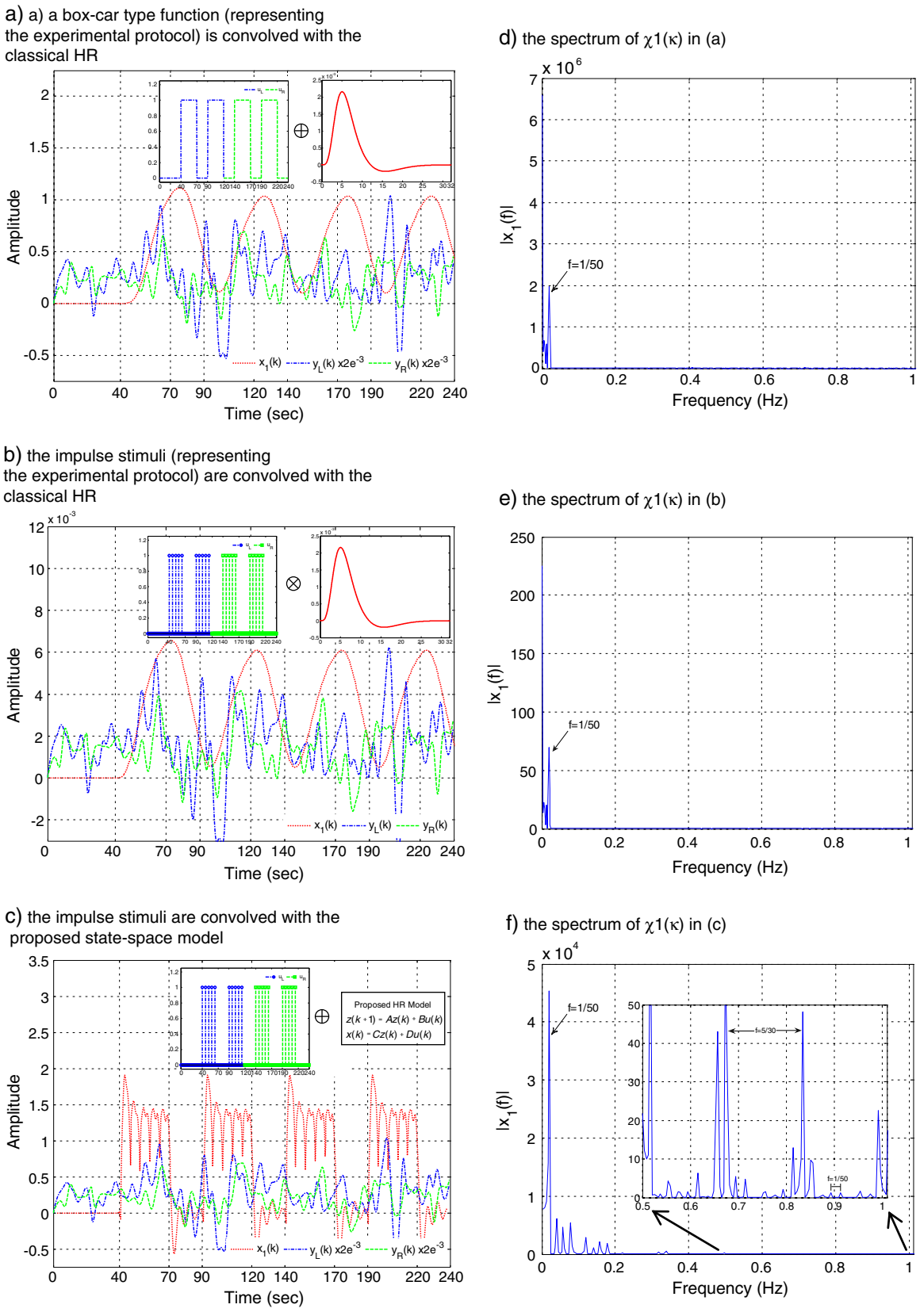

Fig. 12. Comparison of three basis functions, $x_1(k)$, for the MCFG experiment (plotted with the actual HR $y(k)$ measured at an active channel).

Validation results via MCFG experiment

For this experiment, the basis functions generated by the classical method and by the proposed method are drawn in Fig. 12 along with the two real responses $y_L(k)$ and $y_R(k)$ which are observed as active channels at primary left and primary right motor cortexes, respectively. The observed response $y_L(k)$ approximately follows the proposed activity pattern in the first two (right finger grasping) sessions and the observed

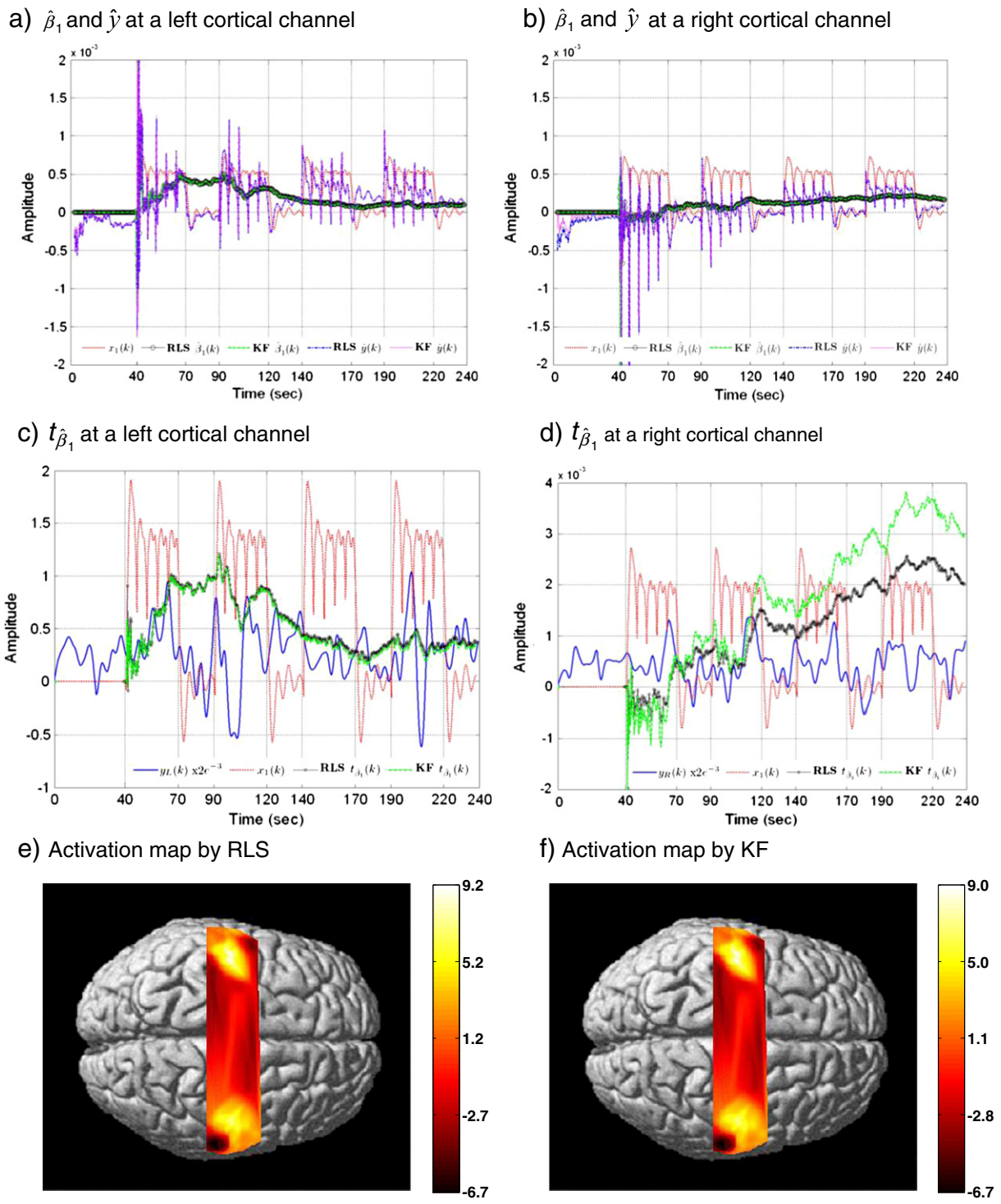

Fig. 13. Results of the MCFG experiment: (a)–(b) recursively extracted activity parameter $\hat{\beta}_1(k)$ and estimated output $\hat{y}(k)$ along with the appropriately scaled modeled response $x_1(k)$; (c)–(d) statistical significance (t-scores) of the activity parameter, $t_{\hat{\beta}_1}(k)$, along with the modeled response $x_1(k)$ and the real responses $y_L(k)$ and $y_R(k)$ observed as active channels at left and right motor-cortexes, respectively; (e)–(f) brain activation maps drawn after the convergence of the activity parameters.

response $y_R(k)$ approximately follows the proposed activity pattern in the last two (left finger grasping) sessions. Thus, it is apparent again that contrary to the classical approach, the proposed model based approach addresses the inter- and intra-activity dynamics of the hemodynamic response. Figs. 13(a) and (b) illustrate the event-related dynamics $\hat{y}^i(k)$ and the activity strength $\hat{\beta}_1(k)$ corresponding to the two appropriate active channels' responses $y_L(k)$ and $y_R(k)$. The statistical significance of these results, plotted in Figs. 13(c–d), demonstrates the effectiveness of the proposed methodology in obtaining the event-related hemodynamic response to neuroactivation. The insignificant values of activity parameters and t-values, estimated with the generalized basis functions, of the nonfunctional cortex's channels reveals the validity for null control. The interpolated brain activation maps are drawn in Figs. 13(e–f) accordingly.

Similar results are obtained with all three subjects with the variations of (i) active channel location and (ii) activity strengths. Channel misalignment during sensor fixation, varied attentiveness, biological- and anatomical-differences, and noise factors are the major sources of these discrepancies. These results demonstrate the effectiveness of the proposed dynamic model (and accordingly the generated basis function for the cortical fNIRS signals) for provision of event-related cortical brain activity along with activity-strength information. This performance, significantly, is superior to that of the classical approach. The crux behind the discrepancy is the dynamic behavior of the proposed HR model for both fast- and slow-switching stimuli. The model utilizes the skills learned for the activation start, stop, and peaking behaviors of the impulse HR instead of using a unique HR or its approximating function.

For demonstration simplicity, the HRF related to HbO is considered and the MBLL is used (but is not restricted to be used) as measurement model (measured photon density to HbO concentration). The proposed method can work equally well with other photon propagation models of HRF measurement, e.g. radiative transfer equation (RTE), diffusion approximation to RTE. The interpolation function $B(r)$ in Eq. (19) is supposed to be three-dimensional in a real measurement scenario (see for example Flexman et al., 2011). But, for optode-coverage manifold of current fNIRS probing, the two-dimensional interpolation function was found to be sufficient to represent the interpolated topographic maps (Abdelnour et al., 2009; Aqil et al., 2012; Ye et al., 2009). The brain-mapping template (left lateral and dorsal views) was depicted using the open-source software SPM8 (Wellcome Department of Cognitive Neurology, London, UK) (Friston et al., 2008). Such *t*-mapping can be drawn to any brain template by proper channel registration with reference points. The experimental data are utilized sample-by-sample to demonstrate the targeted potential for event-related online applications. A real-time framework can be obtained by implementing a recursive framework on parallel processing hardware, like field-programmable gate array (FPGA).

Since the developed model for the demonstration is identified for the primary left motor cortex, the event-related activity detected at the left motor cortex is more prominently detected as compared to the one at the right motor cortex during the MCFG experiment. This is due to the voxel-to-voxel variation of the hemodynamic response to neuroactivation. The proposed method has the potential to investigate precise activity behavior, in that it can address the inter-channel, inter-voxel, and inter-subject variability of hemodynamic behavior by modeling hemodynamic behaviors at all voxels for all the subjects. In this case, the model needs to periodically adapt the subject's intra-channel and intra-voxel hemodynamic variability. Furthermore, the proposed method can be extended to obtain a coupled hemodynamic model to address a broader range of hemodynamic phenomena (like vascular steal, oxygen supply–demand imbalance, cerebral blood flow, cerebral blood volume, and oxygen saturation).

Conclusions

A dynamic model of cortical hemodynamic response was investigated for an impulse RIFT stimulus in order to effectively address the event-related hemodynamic response in addition to inter-activation-block information pertaining to mental tasks. The developed model provides the simple and computationally efficient means of generating the prediction (basis) function for any cortical hemodynamic activation experiment. The variable-pace RIFT and MCFG experiments were conducted with two fNIRS modalities to synthesize the potential of the proposed mechanism. The method was found to outperform the classical method, specifically by preserving the information related to the event-related hemodynamic activity (intra-activation dynamics) in addition to the brain activity status (inter-activation dynamics). Furthermore, the event-related hemodynamic features were extracted by utilizing online algorithms so as to demonstrate the effectiveness of the modeling-based online platforms.

Acknowledgment

This research was supported by the World Class University program funded by the Ministry of Education, Science and Technology through the National Research Foundation of Korea (grant no. R31-20004).

References

Abdelnour, A.F., Huppert, T., 2009. Real-time imaging of human brain function by near-infrared spectroscopy using an adaptive general linear model. NeuroImage 46 (1), 133–143.
Abdelnour, A.F., Schmidt, B., Huppert, T., 2009. Topographic localization of brain activation in diffuse optical imaging using spherical wavelets. Phys. Med. Biol. 54 (20), 6383–6413.
Aqil, M., Hong, K.-S., Jeong, M.-Y., 2011a. Synchronization of coupled chaotic FitzHugh–Nagumo systems. Commun. Nonlinear Sci. Numer. Simul. 17 (4), 1615–1627.
Aqil, M., Hong, K.-S., Jeong, M.-Y., 2011b. Feature extracting design matrix by modeling the hemodynamic behavior of a brain as an LTI system. Conference Proceedings: Annual Meeting of the Organization for Human Brain Mapping, Poster 509-WTh.
Aqil, M., Hong, K.-S., Jeong, M.-Y., Ge, S.S., 2012. Cortical brain imaging by adaptive filtering of NIRS signals. Neurosci. Lett. 514 (1), 35–41.
Boas, D.A., O'Leary, M.A., Chance, B., Yodh, A.G., 1997. Detection and characterization of optical inhomogeneities with diffuse photon density waves: a signal-to-noise analysis. Appl. Opt. 36 (1), 75–92.
Bunce, S.C., Izzetoglu, M., Izzetoglu, K., Onaral, B., Pourrezaei, K., 2006. Functional near-infrared spectroscopy: an emerging neuroimaging modality. IEEE Eng. Med. Biol. Mag. 25 (4), 54–62.
Cope, M., Delpy, D.T., 1988. System for long-term measurement of cerebral blood and tissue oxygenation on newborn-infants by near infra-red trans-illumination. Med. Biol. Eng. Comput. 26 (3), 289–294.
Cui, X., Bray, S., Reiss, A.L., 2010a. Functional near infrared spectroscopy (NIRS) signal improvement based on negative correlation between oxygenated and deoxygenated hemoglobin dynamics. NeuroImage 49 (4), 3039–3046.
Cui, X., Bray, S., Reiss, A.L., 2010b. Speeded near infrared spectroscopy (NIRS) response detection. PLoS One 5 (11), e15474, http://dx.doi.org/10.1371/journal.pone.0015474.
Cui, X., Bray, S., Bryant, D.M., Glover, G.H., Reiss, A.L., 2011. A quantitative comparison of NIRS and fMRI across multiple cognitive tasks. NeuroImage 54 (4), 2808–2821.
Fantini, S., Hueber, D., Franceschini, M.A., Gratton, E., Rosenfeld, W., Stubblefield, P.G., Maulik, D., Stankovic, M.R., 1999. Non-invasive optical monitoring of the newborn piglet brain using continuous-wave and frequency-domain spectroscopy. Phys. Med. Biol. 44 (6), 1543–1563.
Flexman, M.L., Khalil, M.A., Al Abdi, R., Kim, H.K., Fong, C.J., Desperito, E., Hershman, D.L., Barbour, R.L., Hielscher, A.H., 2011. Digital optical tomography system for dynamic breast imaging. J. Biomed. Opt. 16 (7), 076014.
Friston, K.J., Ashburner, J.T., Kiebel, S.J., Nichols, T.E., Penny, W.D., 2008. Statistical Parametric Mapping: The Analysis of Functional Brain Images. Academic Press, Sandiego.
Gallagher, A., Lassonde, M., Bastien, D., Vannasing, P., Lesage, F., Grova, C., Bouthillier, A., Carmant, L., Lepore, F., Béland, R., Nguyen, D.K., 2008. Non-invasive presurgical investigation of a 10 year-old epileptic boy using simultaneous EEG–NIRS. Seizure 17 (6), 576–582.
Haykin, S.S., 2002. Adaptive Filter Theory, 4th edn. Prentice Hall, New Jersey.
Hinds, O., Ghosh, S., Thompson, T.W., Yoo, J.J., Whitfield-Gabrieli, S., Triantafyllou, C., Gabrieli, J.D.E., 2011. Computing moment-to-moment BOLD activation for real-time neurofeedback. NeuroImage 54 (1), 361–368.
Hu, X.-S., Hong, K.-S., Ge, S.S., Jeong, M.-Y., 2010. Kalman estimator- and general linear model-based on-line brain activation mapping by near-infrared spectroscopy. Biomed. Eng. 9 (82), http://dx.doi.org/10.1186/1475-925X-9-82 (Online).
Hu, X.-S., Hong, K.-S., Ge, S.S., 2011. Recognition of stimulus-evoked neuronal optical response by identifying chaos levels of near-infrared spectroscopy time series. Neurosci. Lett. 504 (2), 115–120.
Hu, X.-S., Hong, K.-S., Ge, S.S., 2012. fNIRS based online deception decoding. J. Neural Eng. 9 (2), 1–8.
Li, X., Coyle, D., Maguire, L., McGinnity, T.M., Watson, D.R., Benali, H., 2010. A least angle regression method for fMRI activation detection in phase-encoded experimental designs. NeuroImage 52 (4), 1390–1400.
Ljung, L., 2008. System Identification: Theory for the User, 2nd edn. Prentice-Hall, New Jersey.
Luo, H., Puthusserypady, S., 2007. Estimation of the hemodynamic response of fMRI data using RBF neural network. IEEE Trans. Biomed. Eng. 54 (8), 1371–1381.
Machado, A., Lina, J.M., Tremblay, J., Lassonde, M., Nguyen, D.K., Lesage, F., Grova, C., 2011. Detection of hemodynamic responses to epileptic activity using simultaneous electro-encephalography (EEG)/near infrared spectroscopy (NIRS) acquisitions. NeuroImage 56 (1), 114–125.

Makni, S., Beckmann, C., Smith, S., Woolrich, M., 2008. Bayesian deconvolution of fMRI data using bilinear dynamical systems. NeuroImage 42, 1381–1396.
Markham, J., White, B.R., Zeff, B.W., Culver, J.P., 2009. Blind identification of evoked human brain activity with independent component analysis of optical data. Hum. Brain Mapp. 30 (8), 2382–2392.
Matthews, F., Pearlmutter, B.A., Ward, T.E., Soraghan, C., Markham, C., 2008. Hemodynamics for brain–computer interfaces. IEEE Signal Proc. Mag. 25 (1), 87–94.
O'Leary, M.A., Boas, D.A., Chance, B., Yodh, A.G., 1995. Experimental images of heterogeneous turbid media by frequency-domain diffusing-photon tomography. Opt. Lett. 20 (5), 426–428.
Overschee, P.V., Moor, B.D., 1994. N4SID: subspace algorithms for the identification of combined deterministic-stochastic systems. Automatica 30 (1), 75–93.
Penny, W., Ghahramani, Z., Friston, K., 2005. Bilinear dynamical systems. Philos. Trans. R. Soc. Lond. B Biol. Sci. 360 (1457), 983–993.
Plichta, M.M., Heinzel, S., Ehlis, A.-C., Pauli, P., Fallgatter, A.J., 2007. Model-based analysis of rapid event-related functional near-infrared spectroscopy (NIRS) data: a parametric validation study. NeuroImage 35 (2), 625–634.
Plichta, M.M., Gerdes, A.B.M., Alpers, G.W., Harnisch, W., Brill, S., Wieser, M.J., Fallgatter, A.J., 2011. Auditory cortex activation is modulated by emotion: a functional near-infrared spectroscopy (fNIRS) study. NeuroImage 55 (3), 1200–1207.
Rehan, M., Hong, K.-S., Aqil, M., 2011. Synchronization of multiple chaotic FitzHugh–Nagumo neurons with gap junctions under external electrical stimulation. Neurocomputing 74 (17), 3296–3304.
Stankovic, M.R., Maulik, D., Rosenfeld, W., Stubblefield, P.G., Kofinas, A.D., Drexler, S., Nair, R., Franceschini, M.A., Hueber, D., Gratton, E., Fantini, S., 1999. Real-time optical imaging of experimental brain ischemia and hemorrhage in neonatal piglets. J. Perinat. Med. 27 (4), 279–286.
Viberg, M., 2002. Subspace-based state-space system identification. Circ. Syst. Signal Process. 21 (1), 23–37.
Ye, J.C., Tak, S., Jang, K.E., Jung, J., Jang, J., 2009. NIRS-SPM: statistical parametric mapping for near-infrared spectroscopy. NeuroImage 44 (2), 428–447.
Zhao, H., Tanikawa, Y., Gao, F., Onodera, Y., Sassaroli, A., Tanaka, K., Yamada, Y., 2002. Maps of optical differential pathlength factor of human adult forehead, somatosensory motor and occipital regions at multi-wavelengths in NIR. Phys. Med. Biol. 47 (12), 2075–2093.